Supplementary Information

Photo Switching of Protein Dynamical Collectivity

Mengyang Xu[1], Deepu George[1], Ralph Jimenez[2], Andrea Markelz[1]
[1]University at Buffalo, SUNY, Buffalo, NY, 14260 USA
[2] University of Colorado, Boulder, CO, 80309 USA

Temperatures for the measurements shown in the main text are:
80,100,130,160,180,190,200,205,210,215,220,230,240,250,260,270K

Figure S1 shows the temperature dependent circular dichroism measurements for the unbleached and bleached RFP samples. T_m is most easily attained by the peak in the first temperature derivative of the ellipticity, however in the case of mCherry, the increase in T_m is beyond the measurement range of the CD instrument. In this case the lower bound of the Tm is determined by the midpoint between the low temperature value and the value at 373 K. For all three RFPs, the melting temperature T_m increases with photobleaching. In both photostates the THz net molar absorptivity and low temperature (<200K) resilience follow the thermal stability of the individual proteins.

Figure S2 shows the results for the dipole autocorrelation calculation of the THz absorbance at room temperature. A time-correlation function of the dipole operator relates the dynamics of an equilibrium ensemble to the absorption coefficient. This correlation function reflects the spontaneous fluctuations in the dipole moment and contains information on states of system and broadening due to relaxation. The calculated power spectra by the dipole-dipole autocorrelation function from MD trajectories at room temperature shows the same tendencies as measured: the most flexible TagRFP-T shows the largest calculated THz absorbance, then mOrange2, and mCherry having the smallest calculated absorbance.

Figure S3 shows the improvement in the fitting of the THz absorbance spectra from a simple power law to the sum of two Lorentzians, one centered at 5.3 THz for the known intermolecular water vibration and the second Lorentzian's parameters determined by the fitting. The second Lorentzian typically has a center frequency of 0.6 THz, which agrees well with our quasiharmonic calculation of the intramolecular vibrations of the protein.

Figure S4 shows the fitting parameters extracted using the double Lorentzian fit as described in the main text for mCherry. The solvent dynamical transition T_{DS} is independent of photo state for both mCherry and mOrange2, as was seen for TagRFP-T in the main text. For the photobleached mCherry, the dynamical turn on temperature for the protein increases by ~20K, as was seen for TagRFP-T. The temperature dependence of the low frequency absorbance band of the photobleached state for mOrange2 also substantially changes however rather than just a net shift in T_{DP}, the transition is almost absent, and the temperature dependence appears linear.

Figure S5 shows how changes in the uniformity of the relative B factors correlate with the presence of water channels present in the bleached state of killer Red. Fig. S5 A) and B) show the change in the

structure and relative B factor in the photoactive and bleached states respectively. Figs. S5 C) and D) show the calculated water channels based on these structural measurements. The CAVER software package (1) is applied to calculate the water channels. The calculations find that the water channels substantially increase in the photobleached state as was reported previously in an X-ray crystallographic structure study (2). At the same time we note here that in the structural regions where these channels form, the B-factor uniformity increases, suggesting a stabilization and increase in collectivity in these regions.

Figure S6 shows the fluorescence peak of mOrange as a function of concentration. The peak shifted from ~565 nm to ~610 nm with concentration change of two orders.

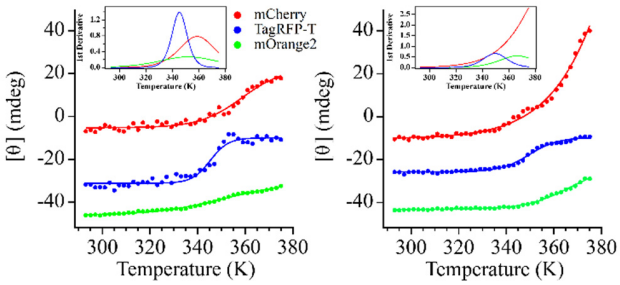

Figure S1. Melting measurements of unbleached A) and bleached B) for mCherry (red), TagRFP-T (blue), and mOrange2 (green) using far-UV CD spectra with sigmoidal fitting ranging from 20°C to 100°C. Insets show the first derivative of the temperature dependence. The peak of the derivative indicates the melting temperature Tm. The values are consistent with the reported T_m = 356K of enhanced green fluorescent protein (EGFP), which has a photostability similar to mOrange2.

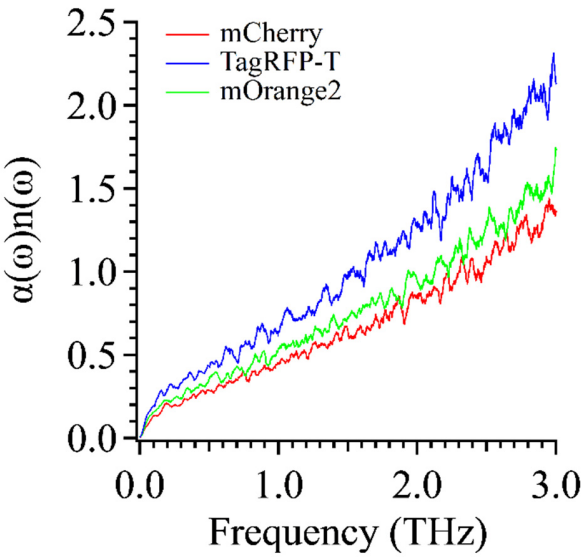

Figure S2. The frequency dependent $\alpha(\omega)n(\omega)$ for mCherry (red), TagRFP-T (blue), and mOrange2 (green) at the same hydration level ($h(g_{water}/g_{protein}) \sim 1.8$), reproduced by dipole-dipole autocorrelation analysis at room termperature within the same THz frequency range of the experiments. The tendency resembles the order of thermal stability.

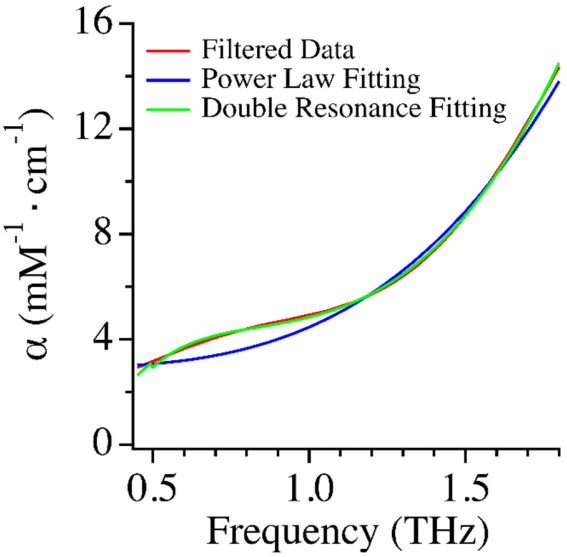

Figure S3. THz molar absorptivity (red) with power-law (blue), and double resonance (green) fittings for unbleached mCherry at 80K.

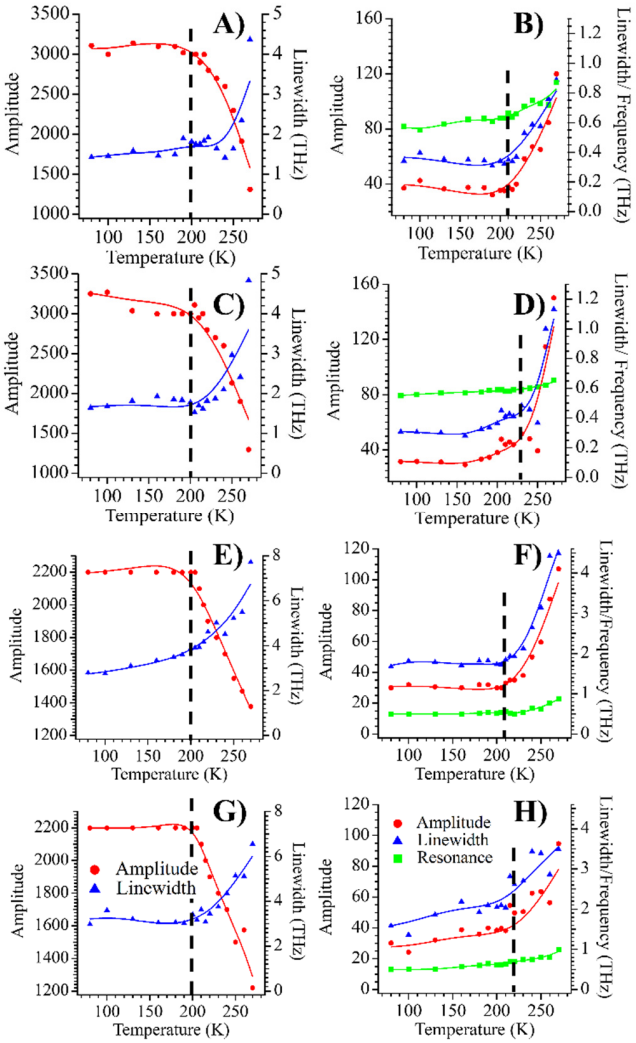

Figure S4. Temperature dependent parameters from double-resonance fitting to terahertz absorbance spectra. mCherry photoactive and photobleached parameters are shown in (A,B) and (C,D) respectively. mOrange2 photoactive and photobleached parameters are shown in (E,F) and (G,H) respectively. The amplitude (red circles) and linewidth (blue trianges) of the 5.3 THz water resonance is shown in the left column (A, C, E and G). The amplitude (red circles), linewidth (blue triangles) and resonant frequency (green squares) for the protein resonant band are shown in the right column (B,D, F and H). The interpolated lines are used as a guide to the eye.

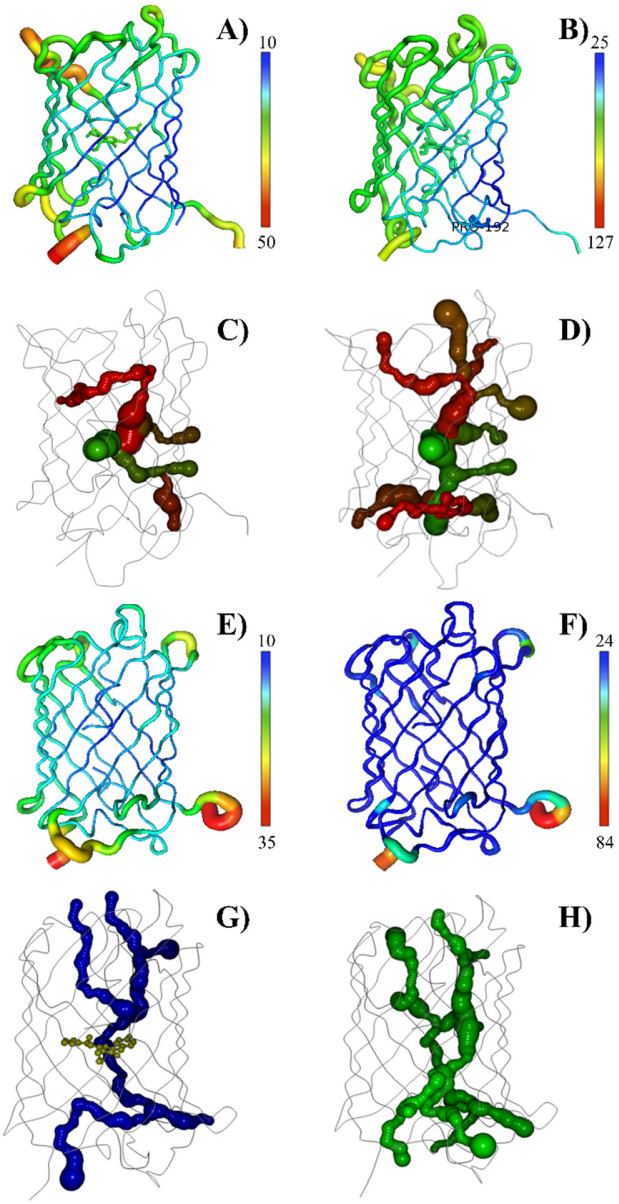

Figure S5. Debye-Waller B factor surface plots for native A) and photobleached B) KillerRED using 2WIQ.pdb and 2WIS.pdb; and for native E) and photobleached F) IrisFP using 2VVH.pdb and 4LJD.pdb. The width and color of the ribbon reflect the average B-value dependent on residues. Note that the colors have been normalized to their average value to focus on relative B-factor distribution. The observed additional water channel gated by Residue 192 is marked in (B). C), D), G) and H) show the water channels calculated by CAVER, corresponding to native and photobleached states for KillerRED and IrisFP, respectively. In both cases, bleached states show additional water channels as well as more uniform B-factor variance.

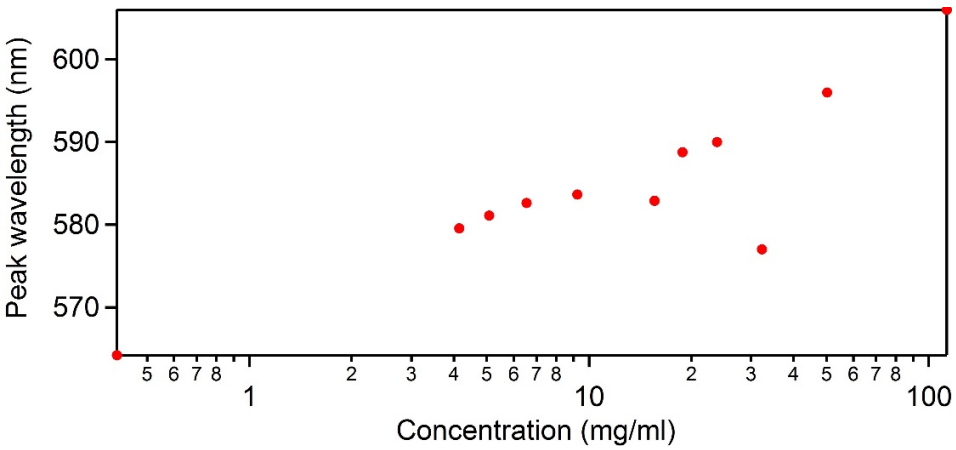

Figure S6. Fluorescence peak of mOrange at room temperature as a function of concentration

1. Chovancova E*, et al.* (2012) CAVER 3.0: A Tool for the Analysis of Transport Pathways in Dynamic Protein Structures. *PLoS Comput Biol* 8(10):e1002708.
2. Carpentier P, Violot S, Blanchoin L, & Bourgeois D (2009) Structural basis for the phototoxicity of the fluorescent protein KillerRed. *FEBS letters* 583(17):2839-2842.